



# Airglow Patches in the Polar Cap Region: A Review

Keisuke Hosokawa<sup>1</sup>  · Ying Zou<sup>2,3</sup> ·  
Yukitoshi Nishimura<sup>2</sup>

Received: 30 April 2019 / Accepted: 18 October 2019 / Published online: 18 November 2019  
© Springer Nature B.V. 2019

**Abstract** Polar cap airglow patches have been known as regions of enhanced 630.0 nm airglow detected by ground-based all-sky imagers at the polar cap latitudes well inside the main auroral oval. Although they were already recognized almost four decades ago as counterparts of polar cap (plasma density) patches, such airglow observations had not been utilized extensively for the studies of ionospheric structures and/or magnetosphere-ionosphere coupling processes in the polar cap. In the last two decades, following the development of highly-sensitive airglow imagers equipped with cooled CCD (Charge Coupled Device) cameras, it has become possible to visualize the dynamical temporal evolution and complicated spatial structure of airglow patches with improved signal-to-noise ratio. Such a progress has enabled us not only to use airglow patches as tracers for plasma convection in the polar cap but also to understand the generation of small-scale plasma irregularities in the ionospheric F region. In addition, recent observations demonstrated a case in which an airglow patch was accompanied by an intense flow channel and corresponding field-aligned current structure along its edges. This implies that airglow patches can signify magnetosphere-ionosphere coupling process in the region of open field lines at the polar cap latitudes, serving as a remote sensing tool just like auroras do. Further studies showed an association of airglow patches with the intensification of aurora on the nightside (Poleward Boundary Intensification: PBI and/or streamer) leading to the expansion phase onset of substorms. This paper

---

Auroral Physics

Edited by David Knudsen, Joe Borovsky, Tomas Karlsson, Ryuho Kataoka and Noora Partmies

---

✉ K. Hosokawa  
[keisuke.hosokawa@uec.ac.jp](mailto:keisuke.hosokawa@uec.ac.jp)

Y. Zou  
[yz0025@uah.edu](mailto:yz0025@uah.edu)

Y. Nishimura  
[toshi16@bu.edu](mailto:toshi16@bu.edu)

<sup>1</sup> Department of Communication Engineering and Informatics, University of Electro-Communications, Tokyo, Japan

<sup>2</sup> Center for Space Physics, Boston University, Boston, USA

<sup>3</sup> Department of Space Science, University of Alabama in Huntsville, Huntsville, USA

reviews such recent progresses in the researches of airglow patches obtained by combining data from all-sky airglow imagers, radars and low-altitude satellite observations in the polar cap.

**Keywords** Airglow · Polar cap · Ionospheric convection · Substorm · Field-aligned currents

## 1 Introduction

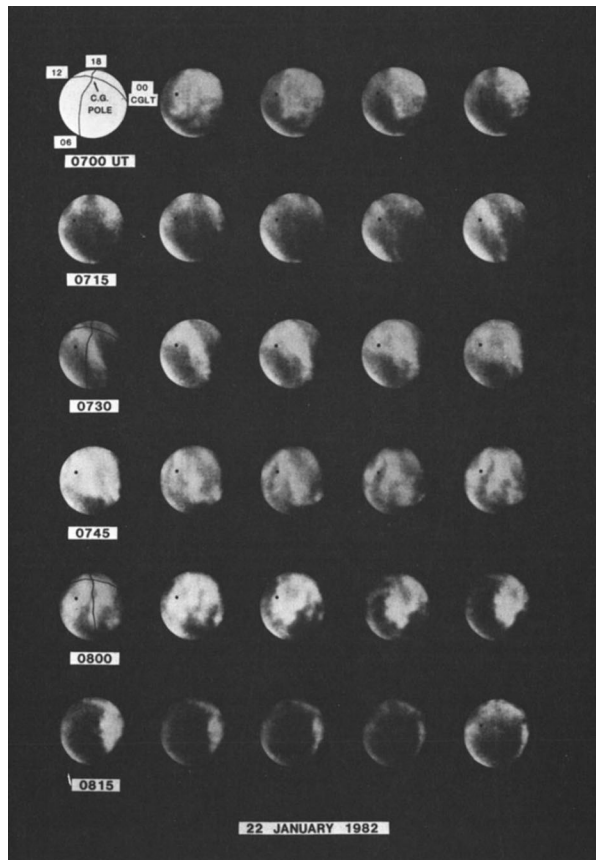
### 1.1 History and Definition

Airglow patches in the polar cap region were first detected by Weber et al. (1984) using all-sky intensified photometers (ASIPs). They were identified in the all-sky images as regions of enhanced airglow at 630.0 nm wavelength, which is known to be proportional to the electron density at the F region altitudes (see Sect. 1.2 for detail). Figure 1 shows a sequence of 630.0 nm airglow patches travelling across the field-of-view of the ASIP. The drift velocity of the airglow patches was anti-sunward (left to right in Fig. 1) and the speed was  $\sim 700 \text{ m s}^{-1}$ , which is consistent with anti-sunward convection in the polar cap during southward IMF conditions. In this example, the 630.0 nm emission intensity was elevated by  $\sim 200$  Rayleigh, which is sub-visible and much darker than typical reddish aurora in the polar cap (Weber and Buchau 1981). Weber et al. (1984) also demonstrated that such enhancements of the 630.0 nm airglow cannot be explained by impact excitation due to soft electron precipitation in the polar cap region. Then, they concluded that the observed airglow patches are not produced by direct particle precipitation, but are primarily airglow structures produced by patches of enhanced F region ionization. In fact, simultaneous ionosonde observations showed that the F region electron density was enhanced by a factor of  $\sim 10$  inside the airglow patches.

Before the first observations of airglow patches by Weber et al. (1984), there had been several radio observations (e.g., ionosonde, total electron content, scintillation etc.) showing periodic enhancements of FoF2, one of the proxies for the F region peak density, at polar cap latitudes (e.g., Weber et al. 1986). Weber et al. (1986) also identified corresponding increases in GPS TEC and amplitude scintillation in satellite signals at VHF and UHF frequencies. These electron density enhancements were named “polar cap patches” which are regions of enhanced electron density travelling from the dayside sunlit region across the central polar cap. The origin of the newly observed airglow enhancements by Weber et al. (1984) was discussed in close connection with the passage of patches of high-density plasma. Specifically, the airglow patches are optical manifestations of polar cap electron density patches. Since the early observations by Weber et al. (1984, 1986), there have been several optical observations in the polar cap showing the two-dimensional structure of polar cap patches (e.g., Fukui et al. 1994; McEwen and Harris 1996; Pedersen et al. 2000; Zhang et al. 2003). Later development of cooled-CCD cameras in the late 90’s enabled us to visualize the detailed spatial structure of airglow patches with much improved signal-to-noise ratio (Dandekar and Bullett 1999; Hosokawa et al. 2006; Carlson et al. 2004). Such recent observations will be introduced in Sect. 1.3.

The definition of polar cap electron density patches is “a region of dense plasma at F region altitudes whose electron density is at least 2 times larger than the surrounding region” (Crowley 1996). This definition has widely been used for detecting electron density patches by using the electron density data from the low-altitude polar orbiting satellites such as DE-2, DMSP, CHAMP and Swarm (Coley and Heelis 1998; Noja et al. 2013; Spicher

**Fig. 1** Successive 630.0 nm airglow images obtained from Thule, Greenland by an ASIP instrument (Weber et al. 1984). The white regions indicate areas of enhanced electron density, which are signatures of polar cap airglow patches. Airglow patches drifted from left (12 MLT) to right (00 MLT) which is anti-sunward direction



et al. 2017). In contrast to electron density patches, there has been no quantitative definition of airglow patches that is used universally. But identification is often easy due to patches' marked difference from auroras in several respects, such as spatial form, characteristic motion, recurrence pattern, and emission wavelengths. Hosokawa et al. (2009b) designed an automatic identification procedure where airglow patches are identified as structures with 630.0 nm emission intensity  $> 30 R$  higher than the background, and with 557.7 nm emission intensity  $< 20 R$  higher (to avoid auroras).

Airglow patches are not auroras, but they are natural optical emissions coming from the atmosphere just like auroras, and their dynamics can be closely related and/or analogized to auroras as seen below. This chapter is mainly focused on progresses made based on optical observations of airglow patches.

## 1.2 Airglow Mechanism

Airglow patches have been observed by using 630.0 nm airglow whose central emission altitude is around 250 km. The process producing this emission can be described by the following two steps reactions (Hays et al. 1978, and references therein):

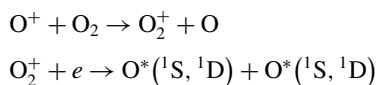
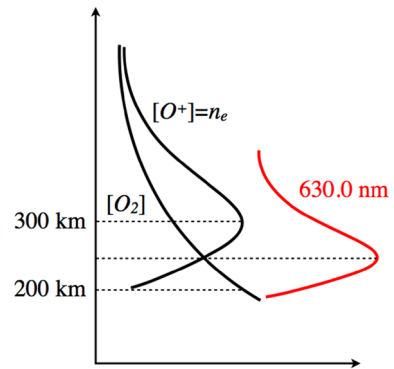
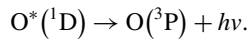


**Fig. 2** Schematic illustration showing the altitude profile of the 630.0 nm airglow emission (red curve). The altitude profile of the densities of atomic oxygen ion ( $\sim$  electron density in the F region) and molecular oxygen (black curves)



The excited state oxygen atom at 1D state was produced by the dissociative recombination through the molecular oxygen atom, which in turn produces emission when it transits to the ground state at  $^3P$  through the following equation:



The emission produced by this process is determined to be 630.0 nm, which is often called red line airglow emission (OI6300).

By looking at the first reaction describe above, the intensity of the emission depends not only on the  $O^+$  density but also on the density of molecular oxygen. The  $O^+$  density is maximized near the peak of F region at around 300 km altitude because they are the dominant ion species at that altitude. The density of neutral oxygen molecule decreases with increasing altitude. This makes the peak of the red line emission slightly below the F region peak altitude (Fig. 2). It depends on the background neutral density conditions (season, local time, and solar wind conditions) as described in Sakai et al. (2014). However, it is mostly located at around 250 km. The emission intensity of 630.0 nm airglow has simply been used as a proxy for the F region electron density (Barbier et al. 1962). As mentioned above, however, the observed emission intensity is also associated with the height distribution of airglow patches. To reduce this effect, much weaker oxygen emission at 777.4 nm (Makela et al. 2001) is sometimes employed for identifying the structure of airglow patches (Carlson et al. 2006). The use of 777.4 nm emission allows us to ignore the effect of molecular oxygen; thus, it provides more direct observations of the electron density at the peak altitude of F region.

In addition to the emission produced through the recombination of cold oxygen ions describe above, thermal excitation is also known to produce the 630.0 nm airglow emission by heat applied to atomic oxygen (Carlson et al. 2013; Kwagala et al. 2017, 2018a, 2018b). Thus, when we examine the 630.0 nm images from ground-based airglow imagers, it is important to distinguish the origins of the airglow emission (recombination or thermal excitation). At least, care must be taken to confirm that the emission is not due to direct impact excitation of oxygen by electrons precipitating from the magnetosphere.

### 1.3 Optical Signature

Optical observations enable a direct visualization of the 2D structure of patches. Patches are often 100–2000 km in size and appear as a circular or cigar-shaped structures. The cigar shape is sometimes elongated in the dawn-dusk direction (Fig. 3a) (Carlson 2003; Hosokawa et al. 2010a, 2013, 2014), and sometimes in the noon-midnight direction (Fig. 3b)



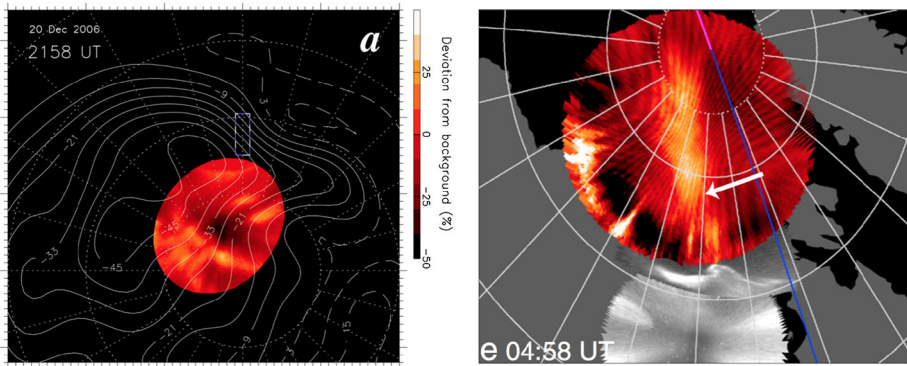


**Fig. 3** Left: an example of dawn-dusk elongated airglow patches in MLT/magnetic latitude coordinates (Hosokawa et al. 2009a). The patch is recorded at 630 nm emission by the OMTI imager at Resolute Bay. Airglow intensity is color-coded according to the percentage deviation from the 1 h running average. Superimposed contours give a pattern of the high-latitude electrostatic potential derived from SuperDARN. Right: an example of noon-midnight elongated airglow patches as marked with the white arrow (Nishimura et al. 2013). The blue and pink lines mark magnetic midnight and noon. The grey-scale images equatorward of the 630.0-nm image are white-light aurora measurements from THEMIS ASIs

(Nishimura et al. 2013; Zou et al. 2015). The specific elongation direction is found to vary with the IMF conditions (Zou et al. 2015), the dawn-dusk elongation occurring under strong IMF  $B_z$  and the noon-midnight elongation under strong IMF  $B_y$ . Factors affecting the elongation direction include how wide the dayside source region of patches is and how much patches rotate within the polar cap (Oksavik et al. 2010). Patches generally have a luminosity of tens to a few hundreds of Rayleighs in the 630.0 nm emission. The luminosity on average decreases as the solar activity declines (McEwen and Harris 1996). It also decreases as patches move away from the dayside cusp (McEwen and Harris 1996). The luminosity has an asymmetric spatial distribution, where the gradient at the patch leading edge is 2–3 times steeper than that at the trailing edge (Hosokawa et al. 2016a). The trailing edge is found to exhibit fingerlike undulations which are likely manifestations of plasma structuring through the gradient-drift instability (GDI) (Hosokawa et al. 2016a) (see details in Sect. 3.1). Such an internal structuring process is also seen in the simultaneous observations of the 630.0 nm emission and incoherent scatter radar observations (Dahlgren et al. 2012a, 2012b). Patches also have faint emissions at 577.7 nm wavelength, the intensity of which is  $< 40\%$  of that of 630.0 nm (McEwen and Harris 1996).

#### 1.4 Motion of Airglow Patches

The motion of airglow patches is controlled by local plasma convection, as found from simultaneous measurements of patches and convection (Fukui et al. 1994; Thomas et al. 2015; Valladares et al. 2015). When convection is sheared, patches are observed to deform accordingly (Hosokawa et al. 2010a). Since convection in the polar cap is governed by the IMF conditions, patch motion is a function of IMF. Statistical analysis finds that the speed of patches increases with the magnitude of the southward IMF  $B_z$  component, and the dawn-dusk component of the patch speed correlates with the IMF  $B_y$  component (Fig. 4) (Zhang et al. 2003; Hosokawa et al. 2009b). When the IMF has a temporal variation, for example turning north from south, patches respond accordingly, stagnating and decaying within the polar cap (Hosokawa et al. 2011).

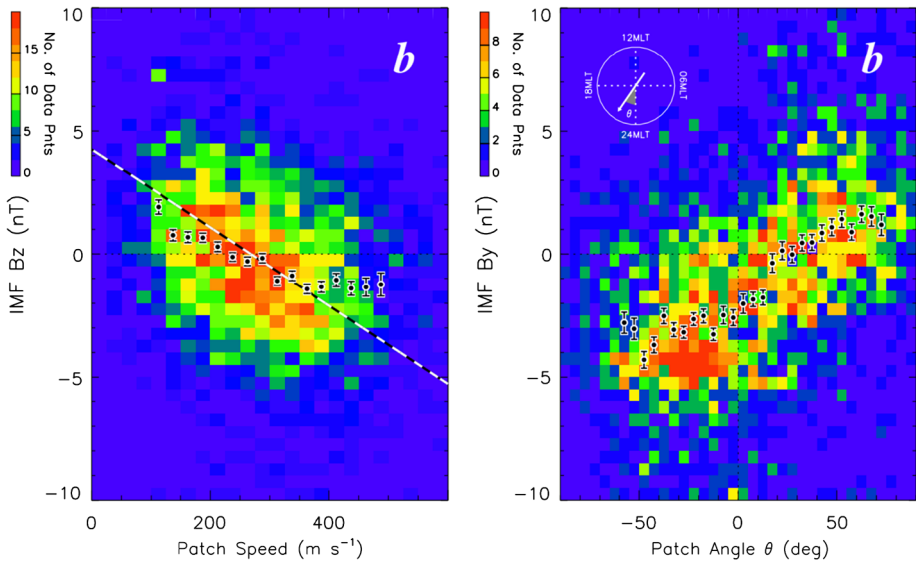


**Fig. 4** Left: Distribution of the speed of patches as a function of the IMF  $B_z$ . The density of data points is self-normalized and shown on a linear scale. The dots and bars represent the mean and standard error of the distributions, respectively, in  $25 \text{ m s}^{-1}$  wide bins of patch speed. Right: Distribution of the moving direction of patches ( $\theta$ : angle of azimuth relative to the noon-midnight line) as a function of the IMF  $B_y$ . The dots and bars represent the mean and standard error of the distributions, respectively, in  $5^\circ$  wide bins of patch speed (Hosokawa et al. 2009b)

One recent finding is that convection in the central polar cap is spatially structured rather than smooth as traditionally assumed. In fact, quite often convection consists of fast-propagating mesoscale structures embedded in a slower convection background and the patch motion is closely related to these mesoscale structures (Nishimura et al. 2014; Zou et al. 2015; Wang et al. 2016; Lyons et al. 2016a). Details of the mesoscale convection will be addressed in Sect. 3.2.

Patches also have vertical motion because the  $\text{ExB}$  convection has a finite vertical projection at regions where magnetic field lines are inclined. Patches thus move upward when convecting towards the pole, and downward when away from the pole. The vertical motion has a direct impact on the luminosity of the patches, causing the luminosity to increase and then decrease during the course of transpolar motion (Perry et al. 2013). Valladares et al. (2015) also showed an example of airglow patches in which their luminosity changed during their transit across the field-of-view of the imager. By reproducing such a situation using Global Theoretical Ionospheric Model (GTIM), they showed that downward neutral wind associated with gravity waves could produce the observed variation of the 630.0 nm emission intensity.

## 2 Dayside Observations

### 2.1 Generation Process

One of the possible sources of airglow patches is high-density plasma in the dayside sunlit region. The high-density plasmas in the source region are captured by the high-latitude con-

vection, in particular the anti-sunward flow near the cusp. During very disturbed conditions, for example during large magnetic storms, the high-latitude convection expands towards lower latitudes and overlaps with the high-density source plasma in the sunlit region. In such cases, high-density plasma, that is as dense as the dayside sunlit region, can be captured and transported towards the central polar cap region as so-called tongue of ionization (TOI: e.g., Sato 1959; Foster et al. 2005). Such a large-scale structure is also observed by an all-sky imager as a huge plume of enhanced 630.0 nm airglow extending in the noon-midnight direction (Hosokawa et al. 2010b). Van der Meeren et al. (2014) also introduced an example of TOI in the 630.0 nm airglow data which stretched all the way across the polar cap from the Canadian dayside sector to Svalbard on the nightside.

The TOI structure has a more continuous spatial shape than patches and are mainly elongated in the noon-midnight direction. However, most of the airglow patches seen in the central polar cap during disturbed conditions are known to be cigar-shaped with elongation more in the dusk-to-dawn direction (Hosokawa et al. 2014). Such a patchy and individual spatial distribution is associated with the temporal variation of the convection on the dayside. In the last 2–3 decades, numerous mechanisms have been proposed for chopping the dayside sunlit plasma into patches: (1) the large-scale direction change in the plasma convection near the cusp due to changes in the IMF  $B_y$  and  $B_z$  (Anderson et al. 1988), (2) plasma density reduction due to convection jets through frictional heating (Valladares et al. 1996); (3) repetitive capturing of the dayside sunlit plasma due to the expansion/contraction of the open/closed field line boundary by transient magnetopause reconnection (Lockwood and Carlson 1992; Carlson et al. 2004, 2006); (4) cutting of high-density plasma by the downward Birkeland current sheet at the equatorward boundary of the flow disturbance (Moen et al. 2006). These proposed mechanisms actually differ from each other. However, all the mechanisms need temporal variations of convection in the vicinity of the dayside inflow region near the cusp. In addition to these mechanisms, impact ionization by soft particle precipitation could also be one of the possible generation mechanisms of polar cap patches (Millward et al. 1999). In particular, it has been pointed out that transient aurora, known as Poleward Moving Auroral Forms (PMAFs: Fasel 1995), plays an important role in producing airglow patches (documented in detail in the next section).

## 2.2 Connection with PMAF

Evidence shows that at least some airglow patches are formed from poleward moving auroral forms (PMAFs). PMAFs are auroral structures that brighten at the equatorward boundary of the dayside auroral oval and propagate poleward into the polar cap (e.g. Sandholt et al. 1986). They are accompanied by fast poleward-directed plasma flows (Milan et al. 1999; Thorolfsson et al. 2000; Oksavik et al. 2004) and are thought to be the optical signature of pulsed reconnection on the dayside magnetopause (Southwood 1987). PMAFs often occur as a series of events separated by a few to ten minutes (Fasel 1995). The occurrence of airglow patches also exhibits periodicity. The periodicity occurs at two distinct periods, 40 min and at 5–12 min (Hosokawa et al. 2013). The larger-period modulations are postulated to result from large-scale reconfiguration of the dayside convection pattern while the shorter-period ones relate to dayside magnetopause reconnection occurring at the same rate as PMAFs.

Observations also directly show that airglow patches can emerge from the most poleward location of PMAFs and continue to propagate poleward (Fig. 5) (Lorentzen et al. 2010; Hosokawa et al. 2016b), even reaching the nightside polar cap and auroral zone (Nishimura et al. 2014). Those patches appear faint, having an intensity less than 150 R in comparison to

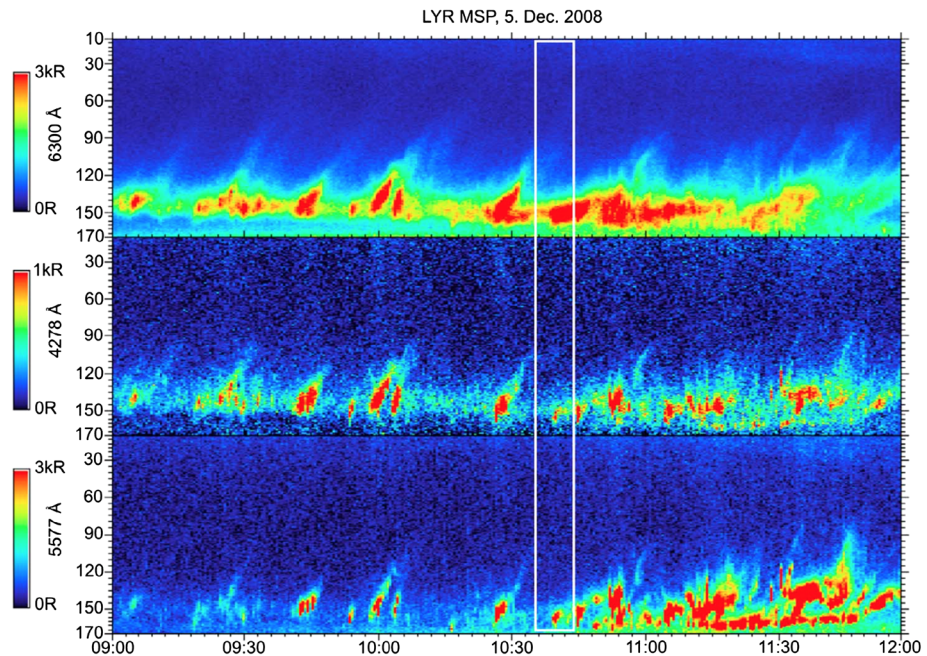


**Fig. 5** 3 wavelength (630.0 nm, 427.8 nm and 557.7 nm) photometer observation of PMAFs and newly created patches (Lorentzen et al. 2010). Only in the 630.0 nm observation (top panel), faint traces of airglow enhancement are seen to emerge from the poleward edge of PMAFs, indicating a nearly one-to-one correspondence between the two features

the typical hundreds-of-Rayleigh patches seen in Hosokawa et al. (2006, 2009b). This fact indicates that the density enhancement within the PMAF-created patches is low. The density enhancement is likely to arise from particle precipitation and/or upwelling of plasma due to Joule heating at lower altitude at the cusp (Lorentzen et al. 2010; Hosokawa et al. 2016b).

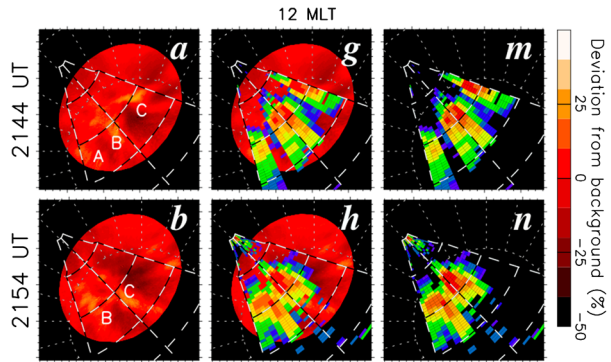
PMAF-created patches are known to cause severe scintillation and resultant loss-of-lock of trans-ionospheric GNSS navigation signals when they are produced on the dayside (Ok-savik et al. 2015). Similar effects on the GNSS signals are detected even when such airglow patches encounter the nightside auroral oval after their travel across the pole (Jin et al. 2014; Van der Meeren et al. 2015). Thus, PMAF-created patches are of particular importance in the framework of space weather.

### 3 Central Polar Cap Observations

#### 3.1 Plasma Structuring

Polar cap patches have been known to be sources of plasma irregularities in the polar cap region. Such small-scale irregularities in the electron density are mainly observed by using coherent scatter radar such as Super Dual Auroral Radar Network (SuperDARN, Chisham et al. 2007). In this case, irregularities are detected as scattering targets of such coherent radars. For example, Milan et al. (2002) showed characteristic poleward moving blobs of backscatter echoes as signatures of polar cap patches. Later, Hosokawa et al. (2009a) demonstrated

**Fig. 6** A sequence of 630.0 nm airglow patches (left panels) and SuperDARN radar backscatter power maps (right panels). In the central panels, superposition of airglow and radar backscatter are shown for comparison (Hosokawa et al. 2009a). The radar echoes are distributed in the entire part of the airglow patches



that radar backscatter echoes were only detected within simultaneously observed airglow patches (Fig. 6). This proves that polar cap patches are active sources of deca-meter scale plasma irregularities.

Past research has suggested plasma irregularities within patches are formed through the so-called gradient-drift instability (GDI: Keskinen and Ossakow 1982). GDI is operative at F region altitudes when the background convection is parallel to the gradient in the electron density. Thus, GDI works only in the trailing edge of patches. In fact, Milan et al. (2002) indicated that the radar backscatter power was relatively larger in the trailing edge of the echo region, which is consistent with the preference of the growth of GDI on the trailing edge. From these observations, GDI has been considered as one of the mechanisms for the internal structuring of plasma within airglow patches. Later, Moen et al. (2012) and Oksavik et al. (2012) demonstrated, by using in-situ electron density measurement by a sounding rocket, that GDI is the primary structuring mechanism of patches in the dayside cusp region. At the same time, Oksavik et al. (2012) pointed out the importance of structured particle precipitation as a source of larger scale “seed” irregularities, which are then efficiently broken down into decameter-scale irregularities by the GDI mechanism. More recent in-situ electron density observations by Goodwin et al. (2015) using the Swarm constellation have suggested that the small-scale internal structure of airglow patches are the product of particle impact ionization in the cusp. On larger spatial scales, GDI can also affect the entire shape of airglow patches. Recently, Hosokawa et al. (2013, 2016a) identified wavy/undulating structure along the trailing edge of airglow patches imaged by high time resolution EMCCD airglow camera (Fig. 7). Such wavy structures are considered to be an indication of GDI as a structuring mechanism of airglow patches.

### 3.2 Flow Channel, Precipitation and FAC

As noted in Sect. 1.4, airglow patches are recently found to be collocated with mesoscale convection structures that are embedded in a slower convection background (Nishimura et al. 2014; Zou et al. 2015; Wang et al. 2016; Lyons et al. 2016a). These patches occur during non-storm time especially under  $B_y$ -dominated IMF conditions. They tend to have a cigar shape that is elongated along or at a small angle from the noon-midnight meridian direction. Since the collocated convection structures have a similarly elongated shape, they are often referred to as flow channels. The flow channels have sharp velocity gradients, particularly at the leading edge of patches. The velocities within the flow channels are usually  $> 200$  m/s larger than the surrounding plasma. Different from the background convection, the flow channels exhibit dynamic evolution even during steady IMF conditions. They may transport



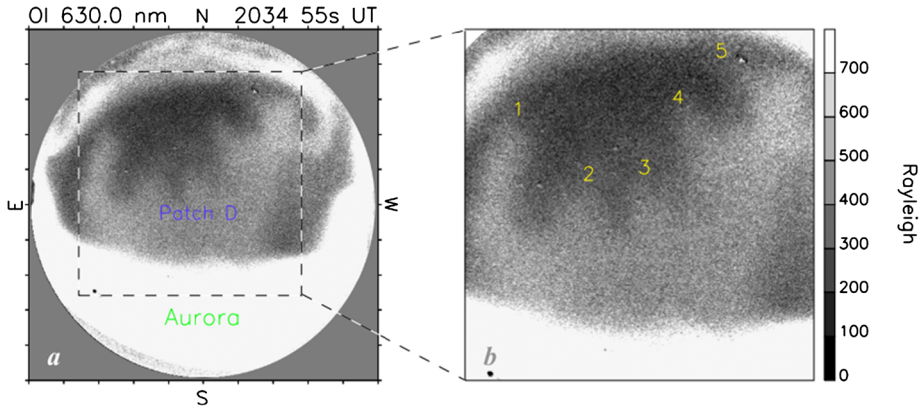


**Fig. 7** 630.0 nm all-sky image of an airglow patch obtained by an all-sky EMCCD camera in Longyearbyen, Norway (Hosokawa et al. 2016b). This airglow patch drifted anti-sunward (from top to bottom in the all-sky field-of-view). In the trailing edge of the airglow patch (top side), intermediate scale (a few tens of kilo-meter) finger-like structures (numbered from 1 to 5) are seen

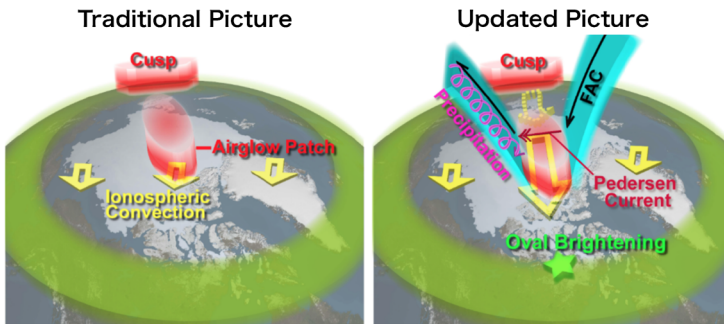
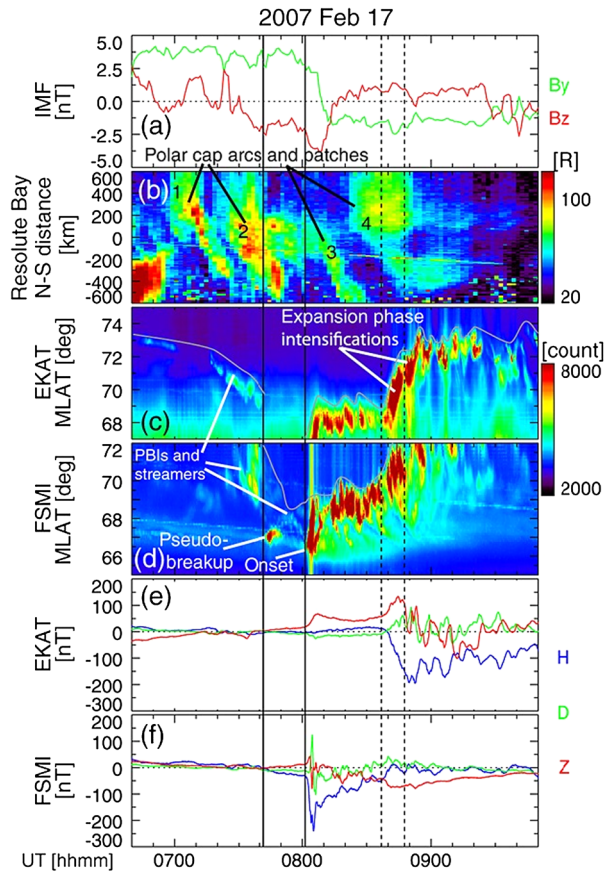


**Fig. 8** Traditional and updated pictures of convection associated with airglow patches (Nishimura and Zou 2017). The green oval denotes the auroral oval and the encircled region is the polar cap. Traditional convection (yellow vectors) is assumed to be smooth and airglow patches (red column) follow large-scale convection. Now patches are realized to be often transported by fast flow channels (larger yellow vectors than surrounding). The channels are associated with FACs (blue sheets) and precipitation (purple helix). FACs are closed through Pedersen currents (red double-arrow). As the channel arrives at nightside auroral oval, oval brightening occurs at the same longitude (Sect. 4). Note that the actual distribution of FACs and precipitation is more complex than shown. There are multiple sheets and the upward FACs and precipitation are often (not always) spread over the patch leading edge

patches all the way to the nightside auroral zone, or may disappear during the course of patch propagation.

The driver of the flow channels is inferred to lie in the magnetospheric lobe based on the fact that they are associated with field-aligned currents (FAC) and soft electron precipitation as shown by the illustration in the right panel of Fig. 8. The left panel presents the scenario if patches follow the smooth background convection. The currents associated with the flow channels are generally weak, being 0.1–0.2  $\mu\text{A}/\text{m}^2$ , and are likely carried by electrons of a few hundred eV (Zou et al. 2016, 2017). They usually exhibit a Region 1 sense, i.e., a downward FAC lying downward of an upward FAC, and can close through Pedersen currents in the ionosphere. The Region 1 sense of FACs is consistent with the locally

**Fig. 9** (a) IMF  $B_y$  and  $B_z$ , keograms of the (b) Resolute Bay, (c) RANK, and (d) SNKQ imagers, and (e) SNKQ magnetometer data (Nishimura et al. 2013). As airglow patches reach the poleward boundary of nightside auroral oval, auroral intensifications subsequently occur



enhanced dawn-dusk electric field across patches. The presence of FACs and particle precipitation implies that the flow channels seen in the ionosphere are driven by processes in the magnetosphere. Specifically, the flow channels are postulated to form during dayside magnetic reconnection. As the reconnected magnetic flux tube propagates anti-sunward away from the dayside reconnection site to the magnetotail, its ionospheric footprint, which is the flow channel, entrains patches across the polar cap. In other words, the evolution of airglow patches corresponds to the evolution of flux tubes formed by the dayside reconnection.

It is noteworthy that not all airglow patches are associated with flow channels and those that are not tend to follow the background convection. It is also likely that not all flow channels are associated with patches. The generation and evolution of the flow channels is not yet understood and requires further investigation.

#### 4 Nightside Observations

Airglow patches exit the nightside polar cap mainly and nearly symmetrically around magnetic midnight (Moen et al. 2007, 2015). One interesting feature recently noted is that as patches exit, auroras within the nightside auroral oval intensify (Lorentzen et al. 2004; Nishimura et al. 2013, 2014). One example is given in Fig. 9. In Fig. 9, four polar cap



structures (which are a mixture of airglow patches and small-scale polar cap arcs) propagated anti-sunward at a speed of  $\sim 500 \text{ m s}^{-1}$ . The first two arrived at the auroral poleward boundary in association with PBI and streamer intensification, which was followed by a pseudobreakup and a substorm marked by the solid vertical lines, respectively. The third and fourth polar cap structures propagated toward the expansion-phase active aurora and they concurred with two major poleward expansions of the auroral oval marked by the dashed vertical lines. This phenomenon echoes observations made with radars where as fast flow channels arrive at the poleward boundary of the nightside auroral oval from the polar cap, poleward boundary intensifications (PBIs) occur (Nishimura et al. 2010; Lyons et al. 2011, 2016b, 2018; Zou et al. 2014). Since airglow patches are commonly associated with flow channels as reviewed in Sect. 3.2, the two observational findings have likely reflected the same physical process.

One key to understanding the relation between patches and auroral intensifications is the timing of intensifications relative to the arrival of patches. This, however, cannot be precisely determined using optical imagers as patches are faint and diffuse. Studies using radars suggest that flow channels statistically arrive right before or simultaneously with the auroral intensifications (Zou et al. 2014). The order of sequence implies that flow channels might trigger auroral intensifications. Currently two different models have been proposed to interpret the causality. One is based on dynamics in the magnetosphere. It is believed that the flow channels correspond to fast flows in the lobe that are  $2\text{--}3 R_e$  wide and that as the lobe flows arrive at the nightside plasma sheet they locally compress the plasma sheet. Magnetotail reconnection then develops and the associated precipitation illuminates auroras (Nishimura and Lyons 2016). The other only concerns ionospheric electrodynamics. As the flow channel approaches the auroral oval, upward and downward FACs are induced at the poleward boundary owing to the sharp gradient of ionospheric conductance. The upward FACs correspond to the observed auroral intensifications (Ohtani and Yoshikawa 2016; Ohtani et al. 2018).

The relation between patches and auroral intensifications has important applications in space weather research, as it is the coexistence of the two that induces strong scintillations in GPS signals (Van der Meeren et al. 2015). One example is given in Fig. 10, which presents the level of phase scintillation at various time instances of a substorm disturbance. Before the substorm onset (Figs. 10a and 10e) phase scintillation was low ( $\sigma_\phi < 0.2$ ) across the entire area under monitoring, including the auroral oval and the southward-propagating airglow patch. As the southwestern edge of the patch approaching the auroral oval, the substorm initiated and the oval expanded poleward. At regions where the patch collocated with the intense auroral emissions, phase scintillation increased to values of  $\sigma_\phi > 1$  (Figs. 10b–10c and 10f–10g). Scintillation at the other portions of the oval remained low. After the expansion subsided and the aurora faded, phase scintillation returned to  $\sigma_\phi < 0.2$ .

## 5 Summary

Polar cap airglow patches were already recognized almost four decades ago as counterparts of polar cap (plasma density) patches. They are the characteristic optical feature of the polar cap under southward IMF condition. However, such airglow observations had not been utilized extensively for the studies of ionosphere in the polar cap, probably due to the limitation in both the spatial and temporal resolutions of optical measurements. In the last two decades, following the development of highly-sensitive airglow imagers equipped with cooled CCD cameras, it has become possible to visualize the dynamical temporal evolution and complicated spatial structure of airglow patches with improved signal-to-noise ratio. Such a

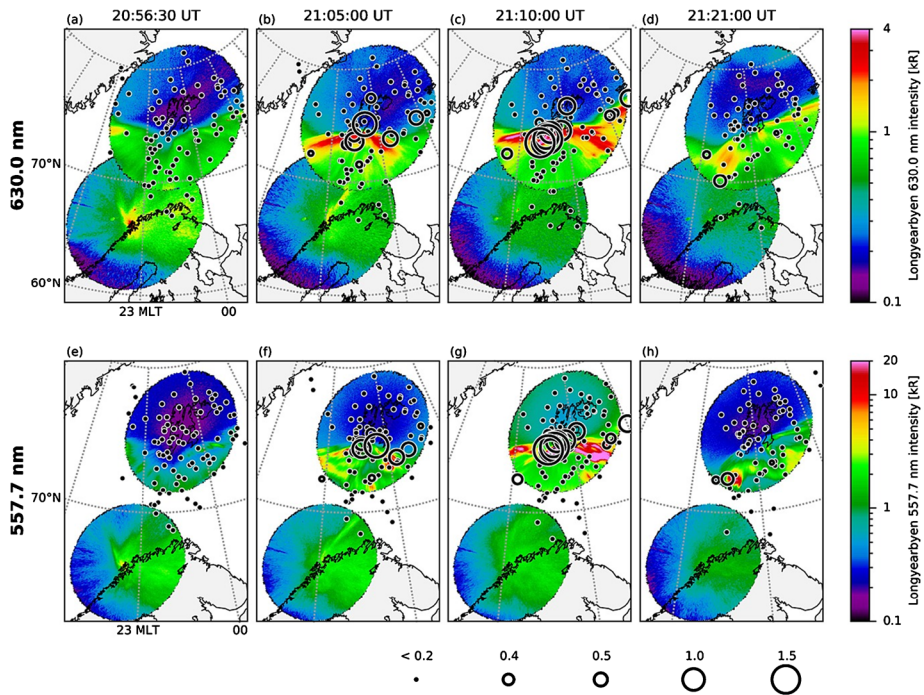


**Fig. 10** Optical emissions and phase scintillation (**a, e**) before, (**b–c** and **f–g**) during, and (**d, h**) after the substorm expansion phase. Panels (**a–d**) and (**e–h**) show red line (630.0 nm) and green line (557.7 nm) emissions, respectively. The GNSS ionospheric piercing points are shown as circles, with the size representing the intensity of the phase scintillation. The arriving patch can be seen in Fig. 3a as a light blue area stretching from west to northeast of Svalbard (Van der Meeren et al. 2015)

progress has enabled us not only to use airglow patches as tracers for plasma convection in the polar cap but also to understand the generation of small-scale plasma irregularities, which are known as backscatter targets for coherent radars and sources of scintillation in the trans-ionospheric satellite signals, through plasma instabilities. In addition, recent observations demonstrated a case in which an airglow patch was accompanied by an intense flow channel and corresponding field-aligned current structure along its edges. This implies that airglow patches can signify magnetosphere-ionosphere coupling process in the region of open field lines at the polar cap latitudes, serving as a remote sensing tool just like auroras do. Further studies showed an association with airglow patches with the intensification of aurora on the nightside (PBI and/or streamer) leading to the expansion phase onset of substorms. In this sense, airglow patches may provide critical clues for discussing the coupling processes between polar cap and the nightside auroral oval, and the onset mechanism of substorms and auroral breakups. In order to facilitate such studies connecting ionospheric and magnetospheric physics, it is highly demanded to combine data from all-sky airglow imagers and radars in the polar cap with those in the auroral zone, and then coordinate multi-instrumental experiments including space-based measurements.

**Acknowledgements** K.H. is supported by JSPS Kakenhi (26302006). Y.Z. is supported by UCAR's Cooperative Programs for the Advancement of Earth System Science (Jack Eddy Postdoctoral Fellowship), and by National Science Foundation (AGS-1664885). Y.N. is supported by NASA grant NNX17AL22G and 80NSSC18K0657, NSF grants PLR-1341359, AGS-1737823, and AFOSR FA9559-16-1-0364.

**Publisher's Note** Springer Nature remains neutral with regard to jurisdictional claims in published maps and institutional affiliations.

## References

- D.N. Anderson, J. Buchau, R.A. Heelis, Origin of density enhancements in the winter polar cap ionosphere. *Radio Sci.* **23**, 513–519 (1988). <https://doi.org/10.1029/RS023i004p00513>
- D. Barbier, F.E. Roach, W.R. Steiger, The summer intensity variations of [OI] 6300 Å in the tropics. *J. Res. Natl. Bur. Stand. D, Radio Propag.* **66D**(1), 145–152 (1962)
- H.C. Carlson, A voyage of discovery into the polar cap and Svalbard, in *Proceedings of the Egeland Symposium on Auroral and Atmospheric Research*, Dep. of Phys., Univ. of Oslo, Norway, ed. by J. Moen, J.A. Holtet (2003), pp. 33–54. ISBN 82-91853-09-6
- H.C. Carlson, K. Oksavik, J. Moen, T. Pedersen, Ionospheric patch formation: direct measurements of the origin of a polar cap patch. *Geophys. Res. Lett.* **31**, L08806 (2004). <https://doi.org/10.1029/2003GL018166>
- H.C. Carlson, J. Moen, K. Oksavik, C.P. Nielsen, I.W. McCrea, T.R. Pedersen, P. Gallop, Direct observations of injection events of subauroral plasma into the polar cap. *Geophys. Res. Lett.* **33**, L05103 (2006). <https://doi.org/10.1029/2005GL025230>
- H.C. Carlson, K. Oksavik, J.I. Moen, Thermally excited 630.0 nm O(<sup>1</sup>D) emission in the cusp: a frequent high-altitude transient signature. *J. Geophys. Res. Space Phys.* **118**, 5842–5852 (2013). <https://doi.org/10.1002/jgra.50516>
- G. Chisham et al., A decade of the Super Dual Auroral Radar Network (SuperDARN): scientific achievements, new techniques and future directions. *Surv. Geophys.* **28**, 33–109 (2007). <https://doi.org/10.1007/s10712-007-9017-8>
- W.R. Coley, R.A. Heelis, Seasonal and universal time distribution of patches in the northern and southern polar caps. *J. Geophys. Res.* **103**(A12), 29,229–29,237 (1998). <https://doi.org/10.1029/1998JA900005>
- G. Crowley, Critical review of ionospheric patches and blobs, in *The Review of Radio Science 1992–1996*, ed. by W. Ross Stone (Oxford University Press, Oxford, 1996)
- H. Dahlgren, J.L. Semeter, K. Hosokawa, M.J. Nicolls, T.W. Butler, M.G. Johnsen, K. Shiokawa, C. Heinselman, Direct three-dimensional imaging of polar ionospheric structures with the Resolute Bay Incoherent Scatter Radar. *Geophys. Res. Lett.* **39**, L05104 (2012a). <https://doi.org/10.1029/2012GL050895>
- H. Dahlgren, G.W. Perry, J.L. Semeter, J.-P. St-Maurice, K. Hosokawa, M.J. Nicolls, M. Greffen, K. Shiokawa, C. Heinselman, Space-time variability of polar cap patches: direct evidence for internal plasma structuring. *J. Geophys. Res.* **117**, A09312 (2012b). <https://doi.org/10.1029/2012JA017961>
- B.S. Dandekar, T.W. Bullett, Morphology of polar cap patch activity. *Radio Sci.* **34**(5), 1187–1205 (1999). <https://doi.org/10.1029/1999RS900056>
- G.J. Fasel, Dayside poleward moving auroral forms: a statistical study. *J. Geophys. Res.* **100**(A7), 11891–11905 (1995). <https://doi.org/10.1029/95JA00854>
- J.C. Foster et al., Multiradar observations of the polar tongue of ionization. *J. Geophys. Res.* **110**, A09S31 (2005). <https://doi.org/10.1029/2004JA010928>
- K. Fukui, J. Buchau, C.E. Valladares, Convection of polar cap patches observed at Qaanaq, Greenland during the winter of 1989–1990. *Radio Sci.* **29**(1), 231–248 (1994). <https://doi.org/10.1029/93RS01510>
- L.V. Goodwin, B. Iserhienrhien, D.M. Miles, S. Patra, C. van der Meeren, S.C. Buchert, J.K. Burchill, L.B.N. Clausen, D.J. Knudsen, K.A. McWilliams, J. Moen, Swarm in situ observations of F region polar cap patches created by cusp precipitation. *Geophys. Res. Lett.* **42**, 996–1003 (2015). <https://doi.org/10.1002/2014GL062610>
- P.B. Hays, D.W. Rusch, R.G. Roble, J.C.G. Walker, The OI (6300 Å) airglow. *Rev. Geophys.* **16**(2), 225–232 (1978). <https://doi.org/10.1029/RG016i002p00225>
- K. Hosokawa, K. Shiokawa, Y. Otsuka, A. Nakajima, T. Ogawa, J.D. Kelly, Estimating drift velocity of polar cap patches with all-sky airglow imager at Resolute Bay, Canada. *Geophys. Res. Lett.* **33**, L15111 (2006). <https://doi.org/10.1029/2006GL026916>
- K. Hosokawa, K. Shiokawa, Y. Otsuka, T. Ogawa, J.-P. St-Maurice, G.J. Sofko, D.A. Andre, Relationship between polar cap patches and field-aligned irregularities as observed with an all-sky airglow imager at Resolute Bay and the PolarDARN radar at Rankin Inlet. *J. Geophys. Res.* **114**, A03306 (2009a). <https://doi.org/10.1029/2008JA013707>
- K. Hosokawa, T. Kashimoto, S. Suzuki, K. Shiokawa, Y. Otsuka, T. Ogawa, Motion of polar cap patches: a statistical study with all-sky airglow imager at Resolute Bay, Canada. *J. Geophys. Res.* **114**, A04318 (2009b). <https://doi.org/10.1029/2008JA014020>

- K. Hosokawa, J.-P. St-Maurice, G.J. Sofko, K. Shiokawa, Y. Otsuka, T. Ogawa, Reorganization of polar cap patches through shears in the background plasma convection. *J. Geophys. Res.* **115**, A01303 (2010a). <https://doi.org/10.1029/2009JA014599>
- K. Hosokawa, T. Tsugawa, K. Shiokawa, Y. Otsuka, N. Nishitani, T. Ogawa, M.R. Hairston, Dynamic temporal evolution of polar cap tongue of ionization during magnetic storm. *J. Geophys. Res.* **115**, A12333 (2010b). <https://doi.org/10.1029/2010JA015848>
- K. Hosokawa, J.I. Moen, K. Shiokawa, Y. Otsuka, Decay of polar cap patch. *J. Geophys. Res.* **116**, A05306 (2011). <https://doi.org/10.1029/2010JA016297>
- K. Hosokawa, S. Taguchi, Y. Ogawa, T. Aoki, Periodicities of polar cap patches. *J. Geophys. Res. Space Phys.* **118**, 447–453 (2013). <https://doi.org/10.1029/2012JA018165>
- K. Hosokawa, S. Taguchi, K. Shiokawa, Y. Otsuka, Y. Ogawa, M. Nicolls, Global imaging of polar cap patches with dual airglow imagers. *Geophys. Res. Lett.* **41**, 1–6 (2014). <https://doi.org/10.1002/2013GL058748>
- K. Hosokawa, S. Taguchi, Y. Ogawa, Edge of polar cap patches. *J. Geophys. Res. Space Phys.* **121**, 3410–3420 (2016a). <https://doi.org/10.1002/2015JA021960>
- K. Hosokawa, S. Taguchi, Y. Ogawa, Periodic creation of polar cap patches from auroral transients in the cusp. *J. Geophys. Res. Space Phys.* **121**, 5639–5652 (2016b). <https://doi.org/10.1002/2015JA022221>
- Y. Jin, J.I. Moen, W.J. Miloch, GPS scintillation effects associated with polar cap patches and substorm auroral activity: direct comparison. *J. Space Weather Space Clim.* **4**, A23 (2014). <https://doi.org/10.1051/swsc/2014019>
- M.J. Keskinen, S.L. Ossakow, Nonlinear evolution of plasma enhancements in the auroral ionosphere. 1. Long wavelength irregularities. *J. Geophys. Res.* **87**, 144 (1982)
- N.K. Kwagala, K. Oksavik, D.A. Lorentzen, M.G. Johnsen, On the contribution of thermal excitation to the total 630.0 nm emissions in the northern cusp ionosphere. *J. Geophys. Res. Space Phys.* **122**, 1234–1245 (2017). <https://doi.org/10.1002/2016JA023366>
- N.K. Kwagala, K. Oksavik, D.A. Lorentzen, M.G. Johnsen, How often do thermally excited 630.0 nm emissions occur in the polar ionosphere? *J. Geophys. Res. Space Phys.* **123**, 698–710 (2018a). <https://doi.org/10.1002/2017JA024744>
- N.K. Kwagala, K. Oksavik, D.A. Lorentzen, M.G. Johnsen, K.M. Laundal, Seasonal and solar cycle variations of thermally excited 630.0 nm emissions in the polar ionosphere. *J. Geophys. Res. Space Phys.* **123**, 7029–7039 (2018b). <https://doi.org/10.1029/2018JA025477>
- M. Lockwood, H.C. Carlson, Production of polar cap electron density patches by transient magnetopause reconnection. *Geophys. Res. Lett.* **19**, 1731–1734 (1992). <https://doi.org/10.1029/92GL01993>
- D.A. Lorentzen, N. Shumilov, J. Moen, Drifting airglow patches in relation to tail reconnection. *Geophys. Res. Lett.* **31**, L02806 (2004). <https://doi.org/10.1029/2003GL017785>
- D.A. Lorentzen, J. Moen, K. Oksavik, F. Sigernes, Y. Saito, M.G. Johnsen, In situ measurement of a newly created polar cap patch. *J. Geophys. Res.* **115**, A12323 (2010). <https://doi.org/10.1029/2010JA015710>
- L.R. Lyons, Y. Nishimura, H.-J. Kim, E. Donovan, V. Angelopoulos, G. Sofko, M. Nicolls, C. Heinselman, J.M. Ruohoniemi, N. Nishitani, Possible connection of polar cap flows to pre- and post-substorm onset PBIs and streamers. *J. Geophys. Res.* **116**, A12225 (2011). <https://doi.org/10.1029/2011JA016850>
- L.R. Lyons, Y. Nishimura, Y. Zou, Unsolved problems: mesoscale polar cap flow channels' structure, propagation, and effects on space weather disturbances. *J. Geophys. Res. Space Phys.* **121**, 3347–3352 (2016a). <https://doi.org/10.1002/2016JA022437>
- L.R. Lyons et al., The 17 March 2013 storm: synergy of observations related to electric field modes and their ionospheric and magnetospheric effects. *J. Geophys. Res. Space Phys.* **121**, 10,880–10,897 (2016b). <https://doi.org/10.1002/2016JA023237>
- L.R. Lyons, Y. Zou, Y. Nishimura, B. Gallardo-Lacourt, V. Angelopoulos, E.F. Donovan, Stormtime substorms: occurrence and flow channel triggering. *Earth Planets Space* **70**, 81 (2018)
- J.J. Makela, M.C. Kelley, S.A. González, N. Aponte, R.P. McCoy, Ionospheric topography maps using multiple-wavelength all-sky images. *J. Geophys. Res.* **106**(A12), 29161–29174 (2001). <https://doi.org/10.1029/2000JA000449>
- D.J. McEwen, D.P. Harris, Occurrence patterns of *F* layer patches over the north magnetic pole. *Radio Sci.* **31**(3), 619–628 (1996). <https://doi.org/10.1029/96RS00312>
- S.E. Milan, M. Lester, S.W.H. Cowley, J. Moen, P.E. Sandholt, C.J. Owen, Meridian-scanning photometer, coherent HF radar, and magnetometer observations of the cusp: a case study. *Ann. Geophys.* **17**, 159–172 (1999)
- S.E. Milan, M. Lester, T.K. Yeoman, HF radar polar patch formation revisited: summer and winter variations in dayside plasma structuring. *Ann. Geophys.* **20**, 487 (2002)
- G.H. Millward, R.J. Moffett, H.F. Balmforth, A.S. Rodger, Modeling the ionospheric effects of ion and electron precipitation in the cusp. *J. Geophys. Res.* **104**(A11), 24603–24612 (1999). <https://doi.org/10.1029/1999JA900249>

- J. Moen, H.C. Carlson, K. Oksavik, C.P. Nielsen, S.E. Pryse, H.R. Middleton, I.W. McCrea, P. Gallop, EIS-CAT observations of plasma patches at sub-auroral cusp latitudes. *Ann. Geophys.* **24**(9), 2363–2374 (2006)
- J. Moen, N. Gulbrandsen, D.A. Lorentzen, H.C. Carlson, On the MLT distribution of *F* region polar cap patches at night. *Geophys. Res. Lett.* **34**, L14113 (2007). <https://doi.org/10.1029/2007GL029632>
- J. Moen, K. Oksavik, T. Abe, M. Lester, Y. Saito, T.A. Bekkeng, K.S. Jacobsen, First in-situ measurements of HF radar echoing targets. *Geophys. Res. Lett.* **39**, L07104 (2012). <https://doi.org/10.1029/2012GL051407>
- J. Moen, K. Hosokawa, N. Gulbrandsen, L.B.N. Clausen, On the symmetry of ionospheric polar cap patch exits around magnetic midnight. *J. Geophys. Res. Space Phys.* **120**, 7785–7797 (2015). <https://doi.org/10.1002/2014JA020914>
- Y. Nishimura, L.R. Lyons, Localized reconnection in the magnetotail driven by lobe flow channels: global MHD simulation. *J. Geophys. Res. Space Phys.* **121**, 1327–1338 (2016). <https://doi.org/10.1002/2015JA022128>
- Y. Nishimura, Y. Zou, *Studying the Auroras and What Makes Them Shine* (Scientia, Bristol, 2017)
- Y. Nishimura et al., Preonset time sequence of auroral substorms: coordinated observations by all-sky imagers, satellites, and radars. *J. Geophys. Res.* **115**, A00I08 (2010). <https://doi.org/10.1029/2010JA015832>
- Y. Nishimura, L.R. Lyons, K. Shiokawa, V. Angelopoulos, E.F. Donovan, S.B. Mende, Substorm onset and expansion phase intensification precursors seen in polar cap patches and arcs. *J. Geophys. Res. Space Phys.* **118**, 2034–2042 (2013). <https://doi.org/10.1002/jgra.50279>
- Y. Nishimura et al., Day-night coupling by a localized flow channel visualized by polar cap patch propagation. *Geophys. Res. Lett.* **41**, 3701–3709 (2014). <https://doi.org/10.1002/2014GL060301>
- M. Noja, C. Stolle, J. Park, H. Lühr, Long-term analysis of ionospheric polar patches based on CHAMP TEC data. *Radio Sci.* **48**, 289–301 (2013). <https://doi.org/10.1002/rds.20033>
- S. Ohtani, A. Yoshikawa, The initiation of the poleward boundary intensification of auroral emission by fast polar cap flows: a new interpretation based on ionospheric polarization. *J. Geophys. Res. Space Phys.* **121**, 10,910–10,928 (2016). <https://doi.org/10.1002/2016JA023143>
- S. Ohtani, T. Motoba, J.W. Gjerloev, J.M. Ruohoniemi, E.F. Donovan, A. Yoshikawa, Longitudinal development of poleward boundary intensifications (PBIs) of auroral emission. *J. Geophys. Res. Space Phys.* **123**, 9005–9021 (2018). <https://doi.org/10.1029/2017JA024375>
- K. Oksavik, J. Moen, H.C. Carlson, High-resolution observations of the small-scale flow pattern associated with a poleward moving auroral form in the cusp. *Geophys. Res. Lett.* **31**, L11807 (2004). <https://doi.org/10.1029/2004GL019838>
- K. Oksavik, V.L. Barth, J. Moen, M. Lester, On the entry and transit of high-density plasma across the polar cap. *J. Geophys. Res.* **115**, A12308 (2010). <https://doi.org/10.1029/2010JA015817>
- K. Oksavik, J. Moen, M. Lester, T.A. Bekkeng, J.K. Bekkeng, In situ measurements of plasma irregularity growth in the cusp ionosphere. *J. Geophys. Res.* **117**, A11301 (2012). <https://doi.org/10.1029/2012JA017835>
- K. Oksavik, C. Meeren, D.A. Lorentzen, L.J. Baddeley, J. Moen, Scintillation and loss of signal lock from poleward moving auroral forms in the cusp ionosphere. *J. Geophys. Res. Space Phys.* **120**, 9161–9175 (2015). <https://doi.org/10.1002/2015JA021528>
- T.R. Pedersen, B.G. Fejer, R.A. Doe, E.J. Weber, An incoherent scatter radar technique for determining two-dimensional horizontal ionization structure in polar cap *F* region patches. *J. Geophys. Res.* **105**(A5), 10637–10655 (2000). <https://doi.org/10.1029/1999JA000073>
- G.W. Perry, J.-P. St-Maurice, K. Hosokawa, The interconnection between cross-polar cap convection and the luminosity of polar cap patches. *J. Geophys. Res. Space Phys.* **118**, 7306–7315 (2013). <https://doi.org/10.1002/2013JA019196>
- J. Sakai, K. Hosokawa, S. Taguchi, Y. Ogawa, Storm time enhancements of 630.0 nm airglow associated with polar cap patches. *J. Geophys. Res. Space Phys.* **119**, 2214–2228 (2014). <https://doi.org/10.1002/2013JA019197>
- P.E. Sandholt, C.S. Deehr, A. Egeland, B. Lybekk, R. Viereck, G.J. Romick, Signatures in the dayside aurora of plasma transfer from the magnetosheath. *J. Geophys. Res.* **91**(A9), 10063–10079 (1986). <https://doi.org/10.1029/JA091iA09p10063>
- T. Sato, Morphology of ionospheric F2 disturbances in the polar regions. *Rep. Ionos. Space Res. Jpn.* **131**, 91 (1959)
- D.J. Southwood, The ionospheric signature of flux transfer events. *J. Geophys. Res.* **92**(A4), 3207–3213 (1987). <https://doi.org/10.1029/JA092iA04p03207>
- A. Spicher, L.B.N. Clausen, W.J. Miloch, V. Lofstad, Y. Jin, J.I. Moen, Interhemispheric study of polar cap patch occurrence based on Swarm in situ data. *J. Geophys. Res. Space Phys.* **122**, 3837–3851 (2017). <https://doi.org/10.1002/2016JA023750>



- E.G. Thomas et al., Multi-instrument, high-resolution imaging of polar cap patch transportation. *Radio Sci.* **50**, 904–915 (2015). <https://doi.org/10.1002/2015RS005672>
- A. Thorolfsson, J.-C. Cerisier, M. Lockwood, P.E. Sandholt, C. Senior, M. Lester, Simultaneous optical and radar signatures of poleward-moving auroral forms. *Ann. Geophys.* **18**, 1054 (2000)
- C.E. Valladares, D.T. Decker, R. Sheehan, D.N. Anderson, Modeling the formation of polar cap patches using large plasma flows. *Radio Sci.* **31**(3), 573–593 (1996). <https://doi.org/10.1029/96RS00481>
- C.E. Valladares, T. Pedersen, R. Sheehan, Polar cap patches observed during the magnetic storm of November 2003: observations and modeling. *Ann. Geophys.* **33**, 1117–1133 (2015). <https://doi.org/10.5194/angeo-33-1117-2015>
- C. Van der Meeren, K. Oksavik, D. Lorentzen, J.I. Moen, V. Romano, GPS scintillation and irregularities at the front of an ionization tongue in the nightside polar ionosphere. *J. Geophys. Res. Space Phys.* **119**, 8624–8636 (2014). <https://doi.org/10.1002/2014JA020114>
- C. Van der Meeren, K. Oksavik, D.A. Lorentzen, M.T. Rietveld, L.B.N. Clausen, Severe and localized GNSS scintillation at the poleward edge of the nightside auroral oval during intense substorm aurora. *J. Geophys. Res. Space Phys.* **120**, 10,607–10,621 (2015). <https://doi.org/10.1002/2015JA021819>
- B. Wang, Y. Nishimura, L.R. Lyons, Y. Zou, H.C. Carlson, H.U. Frey, S.B. Mende, Analysis of close conjunctions between dayside polar cap airglow patches and flow channels by all-sky imager and DMSP. *Earth Planets Space* **68**(1), 150 (2016). <https://doi.org/10.1186/s40623-016-0524-z>
- E.J. Weber, J. Buchau, Polar cap F-layer auroras. *Geophys. Res. Lett.* **8**(1), 125–128 (1981). <https://doi.org/10.1029/GL008i001p00125>
- E.J. Weber, J. Buchau, J.G. Moore, J.R. Sharber, R.C. Livingston, J.D. Winningham, B.W. Reinisch, F layer ionization patches in the polar cap. *J. Geophys. Res.* **89**, 1683 (1984)
- E.J. Weber, J.A. Klobuchar, J. Buchau, H.C. Carlson Jr., R.C. Livingston, O. de la Beaujardiere, M. McCready, J.G. Moore, G.J. Bishop, Polar cap F layer patches: structure and dynamics. *J. Geophys. Res.* **91**(A11), 12121–12129 (1986). <https://doi.org/10.1029/JA091iA11p12121>
- Y. Zhang, D.J. McEwen, L.L. Cogger, Interplanetary magnetic field control of polar patch velocity. *J. Geophys. Res.* **108**, 1214 (2003). <https://doi.org/10.1029/2002JA009742>
- Y. Zou, Y. Nishimura, L.R. Lyons, E.F. Donovan, J.M. Ruohoniemi, N. Nishitani, K.A. McWilliams, Statistical relationships between enhanced polar cap flows and PBIs. *J. Geophys. Res. Space Phys.* **119**, 151–162 (2014). <https://doi.org/10.1002/2013JA019269>
- Y. Zou, Y. Nishimura, L.R. Lyons, K. Shiokawa, E.F. Donovan, J.M. Ruohoniemi, K.A. McWilliams, N. Nishitani, Localized polar cap flow enhancement tracing using airglow patches: statistical properties, IMF dependence, and contribution to polar cap convection. *J. Geophys. Res. Space Phys.* **120**, 4064–4078 (2015). <https://doi.org/10.1002/2014JA020946>
- Y. Zou et al., Localized field-aligned currents in the polar cap associated with airglow patches. *J. Geophys. Res. Space Phys.* **121**, 10,172–10,189 (2016). <https://doi.org/10.1002/2016JA022665>
- Y. Zou, Y. Nishimura, L.R. Lyons, K. Shiokawa, Localized polar cap precipitation in association with nonstorm time airglow patches. *Geophys. Res. Lett.* **44**, 609–617 (2017). <https://doi.org/10.1002/2016GL071168>